MICROSTRUCTURAL OBSERVATIONS OF SPINEL-PYROXENE REFRACTORY INCLUSIONS FROM THE ALHA 77307 CO3.0 CARBONACEOUS CHONDRITE: COMPARISON WITH CAI-LIKE OBJECTS IN AN AMOEBOID OLIVINE AGGREGATE. Jangmi Han[1] and Adrian J. Brearley[1], [1]Department of Earth and Planetary Sciences, MSC03-2040, 1University of New Mexico, Albuquerque, NM 87131, USA. (E-mail: jmhan@unm.edu; brearley@unm.edu).

Introduction: Calcium-Aluminum-rich Inclusions (CAIs) are the oldest solid materials formed in the solar nebula and hence contain a record of the earliest history of our solar system. Extensive studies of CAIs show they are very complex objects that have experienced high-temperature condensation, evaporation, reheating, melting, shock, and secondary mineralization in the solar nebula or on asteroidal parent bodies or both [e.g., 1].

We have commenced a detailed microstructural and microchemical study of CAIs from the ALHA 77307 CO3.0 chondrite using FIB/TEM techniques. The goal of this study is to provide additional constraints on the formation and subsequent thermal processes that have affected CAIs. Here, we report TEM observations of two CAIs and discuss their origin and thermal histories. Additionally, we compare these observations with those from refractory CAI-like objects in an AOA [2,3].

Methods: Individual CAIs from a thin section of ALHA 77307 were identified by elemental X-ray mapping and BSE imaging on a FEI Quanta 3D FEG-SEM/FIB operating at 30kV. Transmission electron microscopy (TEM) sections were prepared from two selected CAIs (#01 and #02) using FIB techniques. The sections were characterized in detail using a variety of TEM techniques, including bright-field TEM, dark- field scanning TEM, electron diffraction, and EDS X-ray analysis using a JEOL 2010F FASTEM FEG scanning TEM operating at 200kV.

Results: A total of ~80 CAIs have been found in one thin section of ALHA 77307. Consistent with previous observations [4], we found two main types of CAIs; (1) spinel-pyroxene inclusions and (2) melilite-rich inclusions. Perovskite is a very common accessory mineral in both CAI types. We also found five spinel-hibonite inclusions, an additional type of inclusion that was not reported by [4].

The two spinel-pyroxene inclusions were studied using SEM and TEM. They are mineralogically-zoned objects that have a spinel core with accessory perovskite enclosed by an outer layer of diopside. CAI #01 (30μm x 40μm in size) consists of a continuous, spinel core surrounded by partial rims of diopside of variable thickness (2-10μm) (Fig. 1a). Similarly, CAI #02 (80μm x 50μm in size) consists of a single spinel core enclosed by a ~10μm-thick diopside layer, followed by a discontinuous forsteritic olivine rim (Fig. 1b). In both inclusions, a discontinuous layer of an intergrowth of spinel and Al-Ti-rich diopside occurs between the spinel core and the diopside rim. In both inclusions, pores of various sizes and shapes occur along the edge of the spinel cores with the Al-Ti-rich diopside layer. These inclusions are texturally and mineralogically similar to spinel-pyroxene inclusions observed in CM2 chondrites [5,6].

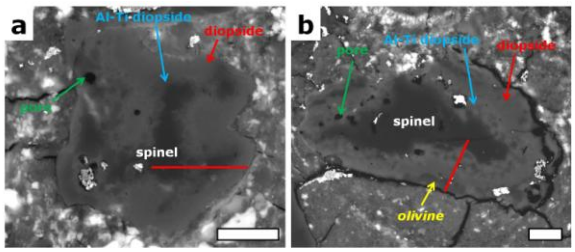

Figure 1. BSE images of (a) CAI #01 and (b) CAI #02, showing mineralogical zonation from a spinel core through a zone of intergrown Al-Ti-rich diopside and spinel and finally a diopside rim. Red bars are the locations of FIB sections. White scale bars are 10μm in length.

TEM observations. A single FIB section from each spinel-pyroxene inclusion was prepared that transected the zonal sequence from the spinel core to the diopside rim. In CAI #02, the section included the outer rim of olivine (Fig. 1b). STEM imaging of the FIB sections show that both inclusions consist of compact aggregates of spinel and diopside with no evidence of pores. A zonal sequence is present consisting of the spinel core followed by an intergrowth of spinel and diopside to the diopside rim, or in the case of CAI #02, the outermost olivine rim (Fig. 2).

The spinel core in both sections consists of polycrystalline aggregates of spinel grains with highly compact and equilibrated microtextures and is not a single spinel crystal, as indicated by SEM BSE images. The outer diopside rim on both inclusions consists of closely-packed aggregates of spinel and diopside. The diopside rim of CAI #01 is a mixture of spinel and diopside with no mineralogical zonation, whereas the diopside rim of CAI #02 has two distinct zones; an inner zone of spinel and diopside and an outer zone with only diopside. The grain boundaries between spinel and diopside are typically embayed and curved. Spinel grain sizes (~0.2-2μm) in the diopside rim are typically smaller than those in the core. In both sections, spinel grains are free of dislocations or defects, but some pyroxene grains contain high densities of dislocations. In pyroxene, dislocations occur as arrays that define subgrain boundaries or linear arrays indicative of deformation followed by high-temperature annealing. Similar dislocation microstructures have been

reported in diopside in Allende Type B1 inclusions [7,8]. The outermost olivine rim in CAI #02 consists of ~1-2μm-sized olivine grains with highly equilibrated grain boundary microtextures, i.e., 120˚ triple junctions (Fig. 2). The olivine grains are also dislocation-free.

In both inclusions, spinel is near $MgAl_2O_4$ and olivine is very close to pure forsterite with ≤ 0.3wt.% FeO. Both minerals are compositionally homogeneous. In contrast, pyroxene from both inclusions shows large variations in MgO, SiO_2, Al_2O_3, and TiO_2, but constant CaO. The Al_2O_3 and TiO_2 contents in pyroxene range from 1 to 32wt.% and from 0 to 15wt.%, respectively. The Al_2O_3 contents in pyroxene from CAI #01 are usually higher than those from CAI #02, although pyroxene from both sections shows similar ranges in TiO_2 content. In general, the Al_2O_3 and TiO_2 contents in pyroxene increase progressively toward the spinel core over a distance of ~10μm. For example, in CAI #02, pyroxene at the interface with the spinel core has 28wt.% Al_2O_3 and 12wt.% TiO_2, whereas pyroxene near the olivine rim contains 1.3wt.% Al_2O_3 and TiO_2 below detection limits. Both sections show the same zonal sequence from spinel, to Al-Ti-rich diopside, and finally Al-Ti-poor diopside towards the CAI rim.

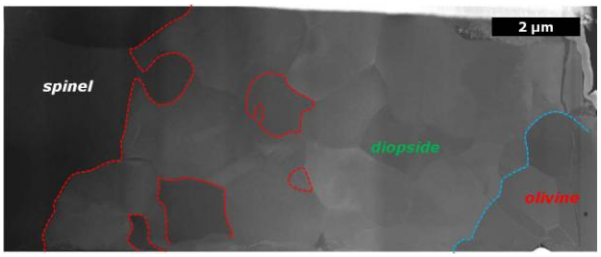

Figure 2. Dark-field scanning TEM image of the section from CAI #02, showing a zonal sequence (from left to right) of the spinel core, the diopside layer, and the outer olivine rim. Spinel grains are outlined in red and olivine in blue.

Comparison with CAI-like objects from an AOA. Our previous SEM and TEM studies on refractory CAI-like objects from an AOA [2,3] are consistent with new observations from two spinel-pyroxene inclusions. The CAI-like objects from the AOA are texturally and mineralogically similar to the spinel-pyroxene inclusions;

- They consist of a zoned sequence with a spinel-rich core, an inner layer of intergrown spinel and Al-Ti-rich diopside, and a diopside rim.
- The FIB sections consist of dense aggregates of spinel and diopside. Embayed and curved grain boundaries between spinel and diopside are common.
- Pyroxene exhibits large variations in chemical composition; generally, pyroxene in the core contains higher Al_2O_3 and TiO_2 contents compared to pyroxene in the rim. Moreover, the Al_2O_3 and TiO_2 contents increase from the rim towards the spinel core.

Discussion: Our TEM observations from two spinel-pyroxene inclusions indicate that their thermal histories are very similar to those experienced by the refractory objects in the AOA. In all the objects, the grain boundary microstructures of the intergrown spinel and pyroxene around the dense spinel core are far from textural and chemical equilibrium. In all these objects, we interpret the embayed character of the spinel core and the corroded appearance of the spinel grains associated with diopside as evidence that spinel has undergone partial reaction to form Al-Ti-rich diopside. The textures and compositions imply that condensate spinel has undergone partial back-reaction with a nebular gas to produce the mineralogically- and compositionally-zoned sequence observed in the inclusions [2,3].

None of the inclusions contain any evidence of primary Ca or Ti-rich phases such as perovskite or melilite coexisting with spinel. These phases could have been completely consumed during reactions with the nebular gas. However, it seems more likely the source of these elements was a partially condensed nebular gas. This is supported by the marked compositional gradients in Ti and Al in the pyroxene outwards from the spinel core. The initial phase of disequilibrium back-reaction of the gas with the spinel produced Al-Ti-rich diopside in a reaction zone on the outer part of the spinel. This zone is represented in the two CAIs by a region of intergrown spinel and Al-Ti-rich diopside. However, as condensation proceeded and the spinel became isolated from the gas phase, condensing diopside became progressively lower in Al and Ti. The preservation of these marked compositional differences in pyroxene compositions indicates that the reactions must have occurred during rapid cooling. Under these conditions, kinetically-controlled condensation processes drove incorporation of Ti into diopside rather perovskite.

Conclusions: The texturally similar refractory CAI-like objects in an AOA and two spinel-pyroxene inclusions preserve a record of gas-solid condensation reactions under highly disequilibrium conditions, probably as a result of fast cooling. Possibly, early condensed solids were transported into a hotter region of the solar nebula that had undergone only partial condensation.

Acknowledgements: This work was funded by NASA grant NNX11AK51G to A. J. Brearley (PI).

References: [1] MacPherson G. J. (1998) *In Treatise on Geochemistry*, pp.201-246. [2] Han J. and Brearley A. J. (2011) *LPS XXXXII*, Abstract #1673. [3] Han J. and Brearley A. J. (2011) *Meteorit. & Planet. Sci., 46*, A87. [4] Russell S. S. et al. (1998) *Geochim. Cosmochim. Acta, 62*, 689-714. [5] MacPherson G. J. and Davis A. M. (1994) *Geochim. Cosmochim. Acta, 58*, 5599-5625. [6] Rubin [7] Barber D. J. et al. (1984) *Geochim. Cosmochim. Acta, 48*, 769-783. [8] Doukhan N. et al. (1991) *Meteoritics, 26*, 105-109.